Title: High metabolism and periodic hypoxia associated with drifting macrophyte detritus in the shallow subtidal Baltic Sea

Author list: Karl M. Attard[1,2,3], Anna Lyssenko[3], Iván F. Rodil[3,4]

Corresponding author: Karl M. Attard karl.attard@biology.sdu.dk

Author affiliations:

[1] Department of Biology, University of Southern Denmark, 5230 Odense M, Denmark

[2] Danish Institute for Advanced Study, University of Southern Denmark, 5230 Odense M, Denmark

[3] Tvärminne Zoological Station, University of Helsinki, J.A. Palménin tie 260, 10900 Hanko, Finland

[4] Department of Biology (INMAR), Faculty of Marine and Environmental Sciences, University of Cádiz, Puerto Real, Spain

Keywords: benthic ecosystems, primary production, respiration, oxygen fluxes, biodiversity

Abstract

Macrophytes form highly productive habitats that export a substantial proportion of their primary production as particulate organic matter. As the detritus drifts with currents and accumulates in seafloor depressions, it constitutes organic enrichment and can deteriorate O_2 conditions on the seafloor. In this study, we investigate the O_2 dynamics and macrobenthic biodiversity associated with a shallow ~2300 m^2 macrophyte detritus field in the northern Baltic Sea. The detritus, primarily *Fucus vesiculosus* fragments, had a biomass of ~1700 g dry weight m^{-2}, approximately 1.5-fold larger than nearby intact *F. vesiculosus* canopies. A vertical array of O_2 sensors placed within the detritus documented that hypoxia ($[O_2] < 63$ µmol L^{-1}) occurred for 23% of the time and terminated at the onset of wave-driven hydrodynamic mixing. Measurements in five other habitats nearby spanning bare sediments, seagrass, and macroalgae indicate that hypoxic conditions were unique to detritus canopies. Fast-response O_2 sensors placed above the detritus documented pulses of hypoxic waters originating from within the canopy. These pulses triggered a rapid short-term (~5 min) deterioration of O_2 conditions within the water column. Eddy covariance measurements of O_2 fluxes indicated high metabolic rates with daily photosynthetic production offsetting up to 81 % of the respiratory demands of the detritus canopy, prolonging its persistence within the coastal zone.

The detritus site had a low abundance of crustaceans, bivalves, and polychaetes when compared to other habitats nearby, likely because their low-O_2 tolerance thresholds were often exceeded.

1. Introduction

Oxygen availability determines ecosystem health and the biogeochemical function of coastal waters (Diaz and Rosenberg, 2008; Middelburg and Levin, 2009; Breitburg et al., 2018). When in gaseous equilibrium with air, seawater typically contains an O_2 concentration ($[O_2]$) between 200-400 µmol L^{-1}, depending on the water temperature and the salinity (Garcia and Gordon, 1992). However, both abiotic and biotic processes cause significant departures from equilibrium. The main source of O_2 to coastal waters is the atmosphere, where the diffusion of O_2 is governed by the air-to-sea gas exchange rate (Berg and Pace, 2017; Long and Nicholson, 2018). In shallow waters and light-exposed seafloor sediments, O_2 is produced by primary producers as a by-product of photosynthesis, and it is consumed by consortia of microbes and fauna directly, through aerobic respiration, and indirectly, through the oxidation of reduced substances (Glud, 2008). If O_2 consumption exceeds supply for a sufficiently long period, O_2 conditions deteriorate and become hypoxic ($[O_2] < 63$ µmol L^{-1}). Hypoxia is becoming more common, more intense, and is affecting larger areas of coastal waters, increasingly placing ecosystems and the services they provide at risk (Breitburg et al., 2018). There are several well-known variants of coastal hypoxia (Diaz and Rosenberg, 2008; Carstensen and Conley, 2019). Seasonal hypoxia, the most common form, typically occurs in summer when warm waters, strong stratification, and high organic enrichment combine to deplete O_2 until autumn (Robertson et al., 2016). Periodic hypoxia, in contrast, occurs more often due to local weather dynamics and tidal cycles but individual events are shorter (Diaz and Rosenberg, 1995), whereas diel cycles with large day-to-night $[O_2]$ excursions trigger hypoxia for a few hours daily (Davanzo and Kremer, 1994; Tyler et al., 2009). All events are expected to affect biodiversity and biogeochemical cycling to varying degrees. Seasonal and periodic hypoxia are associated with large-scale mortality of organisms and a switch between retention and removal of bioavailable nutrients such as nitrate, ammonium, phosphate, and toxic hydrogen sulfide (Middelburg and Levin, 2009; Carstensen and Conley, 2019). Short-term hypoxia can similarly exceed lethal and non-lethal thresholds for many taxa (Vaquer-Sunyer and Duarte, 2008), although, due to their sporadic nature, their occurrence and impacts are less understood.

Given the importance of O_2 in coastal waters, $[O_2]$ is one of the most frequently measured environmental parameters. Near-seabed $[O_2]$ is typically measured using long-term stable O_2

sensors (e.g. optodes) (Bittig et al., 2018) that are moored ~0.3-1.0 m above the seafloor, or by performing vertical profiles of water column [O_2] down to ~1.0 m above the seafloor using multiparameter sondes. National monitoring programs such as those maintained by the Swedish Meteorological and Hydrological Institute and the Finnish Environment Institute provide a wealth of essential open-access data, enabling important analyses detailing the prevalence and intensity of coastal hypoxia (Virtanen et al., 2019; Conley et al., 2011; Carstensen and Conley, 2019). Notwithstanding the progress being made in coastal monitoring, it was demonstrated more than 40 years ago that the largest [O_2] gradients may occur just a few cm above the seafloor due to the high reactivity of marine sediments and a strong benthic O_2 demand (Jorgensen, 1980). To date, records of hypoxia in the shallow subtidal zone are still somewhat scarce. In a compilation of monitoring data for the northern Baltic Sea (Gulf of Finland and Archipelago Sea), Virtanen et al. (2019) found that just 11 out of 461 (or 2.4%) of the monitoring stations that registered hypoxia occurred in waters < 5 m depth. While this may reflect a true signal that hypoxia is more widespread in deeper coastal waters, it is also likely that hypoxic conditions go undetected if measurements are performed away from the seafloor, as is common practice (Conley et al., 2011; Virtanen et al., 2019).

Around two-thirds of the ocean's photosynthetic biomass is bound in macrophytes growing in shallow waters along the world's coastline (Smith, 1981). Through seasonal decay, epiphyte growth, grazing, and physical forcing (e.g. waves, currents, ice scouring), macrophytes export a large proportion of their primary production (~40 %) to their surroundings as detritus (Attard et al., 2019a; Krumhansl and Scheibling, 2012; Duarte and Cebrián, 1996). Macrophyte detritus drifts with the currents and accumulates on the shoreline and in low-energy marine environments (e.g. shallow seafloor depressions and in deeper waters), where it constitutes habitat structure and organic enrichment to the receiving habitat (Norkko and Bonsdorff, 1996b). Given high enough abundance, detritus suppresses the diffusion of O_2 from the water column to the sediment surface and it exacerbates O_2 depletion on the seabed as it decays. Large accumulations of unattached ephemeral macroalgae such as the brown algae *Ectocarpus siliculosus* and *Pylaiella littoralis* are common in eutrophic coastal waters such as the Baltic Sea, forming thin mats above the seafloor typically a few centimeters thick (Norkko and Bonsdorff, 1996a). While coastal hypoxia is most commonly associated with eutrophic waters such as the Baltic Sea (Carstensen and Conley, 2019; Conley et al., 2011), hypoxic (and even sulfidic) conditions have been reported in remote and more pristine environments such as the high Arctic due to large accumulations of detritus produced from

92 perennial brown seaweeds (Glud et al., 2004). However, the O_2 dynamics within accumulations of
93 drifting detritus and the potential implications for the associated fauna remain poorly understood.
94 Understanding the ecological and biogeochemical implications of drifting macrophyte detritus is
95 particularly important given the ambitions to vastly increase macroalgal farming (Broch et al.,
96 2019), which would result in increased deposition of macrophyte detritus on the coastal seafloor
97 (Broch et al., 2022).

98 In this study, we investigate the O_2 dynamics and macrobenthic biodiversity associated with a
99 shallow ~2300 m^2 macrophyte detritus field composed of *Fucus vesiculosus* fragments in the
100 northern Baltic Sea. To assess O_2 production versus consumption rates of the detritus canopy, we
101 deployed an eddy covariance system on multiple occasions to extract benthic O_2 fluxes non-
102 invasively. Using a vertical array of O_2 sensors and an acoustic velocimeter, we monitored O_2
103 distribution within the canopy and the hydrodynamics above the canopy to assess the occurrence
104 and intensity of hypoxic events and their links to local hydrodynamics. We performed biodiversity
105 surveys to identify the prevailing taxa, and we compared hypoxic thresholds of these taxa to [O_2]
106 measured *in situ* to identify potential stress. Measurements were also performed in five other
107 habitats nearby spanning bare sediments, seagrass, and macroalgae for comparison.

108 ## 2. Materials and Methods

109 ### *2.1. Study location*

110 The study was performed in the microtidal Baltic Sea nearby the Tvärminne Zoological Station in
111 SW Finland. Although the focus of our study was to investigate drifting macrophyte detritus, we
112 selected an additional five study sites within the shallow subtidal zone (2-4 m depth) for
113 comparison, representing key habitats in the Baltic Sea: one site with bare sediments, two sites with
114 seagrass (predominantly *Zostera marina*; sheltered and exposed), and two sites with intact
115 macroalgae canopies (predominantly *Fucus vesiculosus*; sheltered and exposed) (Table 1).

Site	Location	Deployment start	Deployment duration (h)	Water depth (m)	Water temperature (°C)	Minimum O_2 (µmol L^{-1})	Maximum O_2 (µmol L^{-1})	Hypoxia duration (h)
Macrophyte detritus	59 811613 N 23 206624 E	29-05-2018	120	3.0	12	0.6	429	27
Bare sediments	59 841532 N 23 253370 E	20-05-2018	96	3.7	11	307	407	0
Sheltered *Z. marina*	59 841551 N 23 251203 E	27-05-2018	87	4.0	16	272	333	0

Exposed *Z. marina*	59 827008 N 23 151976 E	08-06-2018	120	2.9	10	281	437	0
Sheltered *F. vesiculosus*	59 826856 N 23 209721 E	08-06-2018	120	2.0	10	253	489	0
Exposed *F. vesiculosus*	59 811359 N 23 207281 E	31-05-2018	116	2.0	9	287	427	0

Table 1: Environmental conditions and low-oxygen events at the six study sites

2.2. [O_2] dynamics in benthic habitats

To investigate the near-bed [O_2] dynamics and its environmental controls, we equipped a tripod frame with a suite of sensors consisting of three cross-calibrated dissolved [O_2] loggers with inbuilt temperature compensation (HOBO U26-001, Onset), a 6 MHz acoustic velocimeter (Vector, Nortek), a photosynthetic active radiation (PAR) sensor (RBRsolo with Licor PAR Quantum 192SA), and a saltwater conductivity sensor (HOBO U24-002-C). The [O_2] loggers have a factory-specified accuracy of ± 6 µmol L^{-1} from 0 to 250 µmol L^{-1}, ± 16 µmol L^{-1} from 250-625 µmol L^{-1}, a resolution of 0.6 µmol L^{-1} and a 90% response time (T_{90}) < 2 min. The [O_2] and conductivity sensors were mounted onto a 75 cm-long stainless-steel rail affixed to the tripod leg (Fig. 1). The sensors were secured to the rail at various heights above the seabed using rail mount clamps. For the study sites with canopies, two sensors were set inside the canopy; one sensor was ~5 cm above the seafloor and one was close to the top of the canopy (15-25 cm). The third sensor was placed in the water above the canopy (~35 cm above the seafloor). The tripod was deployed by divers from a small boat and was carefully positioned on the seafloor using a lift bag. The exact sensor heights were noted by the divers once the instrument was on the seafloor. The instrument was left to record data for 3-5 days at each site. The velocimeter sampled three-dimensional flow velocity continuously at 8 Hz, whereas the [O_2], temperature, conductivity, and PAR sensors recorded data every minute.

To investigate [O_2] dynamics and its environmental drivers, all sensor time series were aligned in time and analyses were performed to investigate vertical gradients in O_2 distribution, diel [O_2] excursions, and boundary-layer hydrodynamics. We assessed the occurrence of hypoxia ([O_2] < 63 µmol L^{-1}) by quantifying the magnitude (lowest [O_2] value) and the duration (in hours) of hypoxic events. The high-frequency velocity data were used to calculate mean flow velocity magnitude ($\overline{U}$) as the sum of streamwise (u) and traverse (v) components, as $\overline{U} = \sqrt{u^2 + v^2}$.

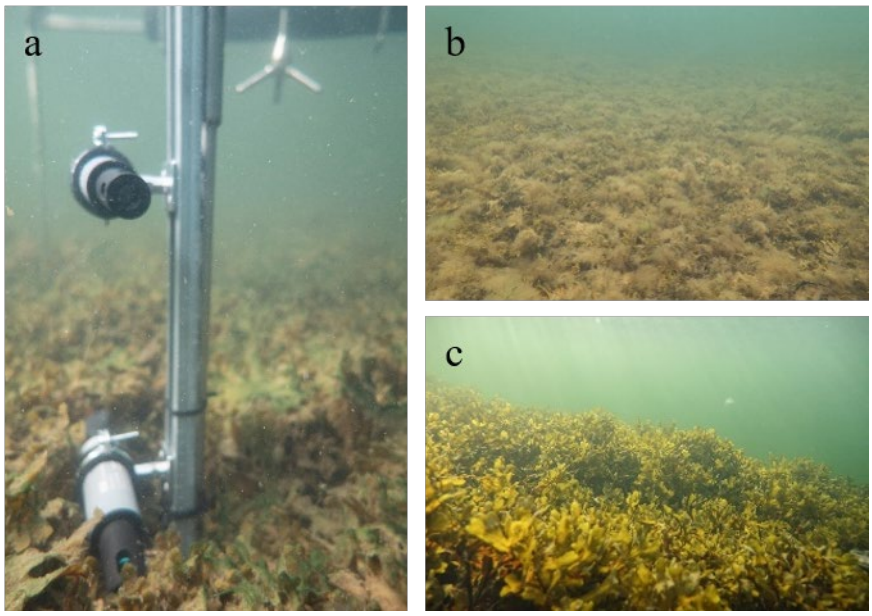

Fig. 1: The study area showing (a) the instrument deployed within the detritus canopy, (b) a broad-scale view of the detritus accumulation area, and (c) a nearby intact *Fucus vesiculosus* canopy.

2.3. Benthic O_2 fluxes

An aquatic eddy covariance system was deployed at the detritus site to quantify benthic O_2 fluxes at the canopy-water interface on three occasions (June 2017, September 2017, and May 2018). Eddy covariance integrates over a relatively large seafloor area (typically ~30 m^2) (Berg et al., 2007), and extracts fluxes without disturbing the hydrodynamics or the light, which is particularly useful when trying to understand the mechanistic drivers of [O_2] dynamics (Berg et al., 2022). The eddy covariance setup was identical to the tripod frame described above, with the addition of a fast-response (T_{90} < 0.3 s) [O_2] microsensor setup for covariance measurements (McGinnis et al., 2011). The hardware and data processing techniques are described in detail in Attard et al. (2019b). This instrument can capture the entire range of flux-contributing turbulent eddies within the benthic boundary layer, and this information is used to approximate the benthic O_2 flux non-invasively (Berg et al., 2003; Berg et al., 2022). The instrument recorded co-located measurements of the vertical velocity (w) and the O_2 concentration (C) at 32 Hz, and the data were processed using a multiple-step protocol detailed in Attard et al. (2019b) to extract and quality-check benthic fluxes. In short, the data streams for w and C were decomposed into mean and fluctuating components using Reynolds decomposition, as $w = \bar{w} + w'$ and $C = \bar{C} + C'$ (Berg et al., 2003). The turbulent flux (J_{EC}) was then computed in units of mmol O_2 m^{-2} h^{-1} as $J_{EC} = \overline{w'C'}$, where the overbar

represents a period of 15 min. The turbulent flux was then summed with a storage correction term to calculate the total benthic flux ($J_{benthic}$, mmol O_2 m^{-2} h^{-1}) (Rheuban et al., 2014), as:

$$J_{benthic} = J_{EC} + \int_0^h \frac{\partial C}{\partial t} \mathrm{d}z$$

The storage correction term was defined using the three [O_2] optodes placed within and above the canopy. For the correction, we defined a matrix with the number of rows *n* corresponding to the sensor measurement height above the seafloor (1 row per cm) (Camillini et al., 2021). To do this, the oxygen time series, consisting of [O_2] measurements performed at three heights within the canopy, were converted to a matrix using the software package OriginPro 2022. Since the measurement height of the three sensors were spaced nonlinearly, the data were first converted to XYZ column format using the w2xyz function. Next, the three rows, representing the [O_2] time series measurements at three heights, were expanded to *n* rows, with *n* representing the sensor measurement height in cm (from 0 to *n* cm above seabed, 1 row per cm) using the XYZ Gridding function. This generated a matrix of *n* rows consisting of linearly interpolated [O_2]. Interpolation was performed using the Random (Renka Cline) gridding method. Next, a storage correction term was calculated for each 1 cm cell as described by Rheuban et al. (2014), and the total storage correction was subsequently computed for the water volume below the sensor measurement height as the sum of the *n* rows. The high-frequency [O_2] time series from the fast-response microsensors were also analyzed to identify any pulses of low [O_2] waters originating from within the canopy and propagating upwards into the water column.

2.4. Benthic metabolic rates

The O_2 flux time series was separated into individual 24 h periods (midnight to midnight). The daytime flux ($Flux_{day}$, mmol O_2 m^{-2} h^{-1}) was computed as a bulk average of fluxes measured when PAR > 1.0 µmol m^{-2} s^{-1}. The nighttime flux ($Flux_{night}$, mmol O_2 m^{-2} h^{-1}) was calculated as the average of the remaining fluxes, when PAR < 1.0 µmol m^{-2} s^{-1}. These two values and the number of daylight hours (h_{day}) were used to estimate the daily photosynthetic rate, termed the gross primary production (*GPP*, in mmol O_2 m^{-2} d^{-1}), as $GPP = Flux_{day} + abs(Flux_{night}) * h_{day}$, and daily respiration (*R*, in mmol O_2 m^{-2} d^{-1}), as $R = abs(Flux_{night}) * 24$, assuming a light-independent respiration rate. The latter is a common assumption, but it is known that it underestimates the true metabolic activity (Fenchel and Glud, 2000; Juska and Berg, 2022). The daily balance between

191 *GPP* and *R*, termed the net ecosystem metabolism (*NEM*, in mmol O_2 m^{-2} d^{-1}) was estimated as
192 $NEM = GPP - R$ (Attard et al., 2019b).

193 The relationship between seafloor PAR and the in situ benthic O_2 flux was investigated using light-
194 saturation curves. Hourly O_2 fluxes were plotted against the corresponding near-bed incident PAR
195 and the relationship between the two was investigated using a modified tangential hyperbolic
196 function by Platt et al. (1980), as $O_2\ flux = P_m * \tanh\left(\frac{\alpha I}{P_m}\right) - R$, where P_m is the maximum rate of
197 hourly gross primary production, α is the initial quasi-linear increase in O_2 flux with PAR, I is near-
198 bed irradiance (PAR), and R is the dark respiration rate. The photosaturation parameter, I_k (µmol
199 PAR m^{-2} s^{-1}) was derived as P_m/α. Non-linear curve fitting was performed in OriginPro 2022 using
200 a Levenberg–Marquardt iteration algorithm, until a Chi-Squared tolerance value of 1E-9 was
201 reached (Attard and Glud, 2020).

202 *2.5. Biodiversity sampling*

203 At all six sites, we aimed to obtain a quantitative understanding of the abundance, biomass, and
204 species richness of macrophytes and macrofauna (infauna and epifauna). The different habitats
205 required different sampling strategies, since four sites were sedimentary (bare sediments site, two
206 seagrass sites, and the detritus sites) and two sites were rocky (two macroalgal sites) (Rodil et al.,
207 2019).

208 At the time of our study, the detritus site had a ~20-cm thick detritus mat covering the seabed
209 sediments. The detritus canopy was sampled using large stainless steel core liners (inner diameter =
210 19 cm; n = 4) capable of cutting through the mat, and the collected samples were transferred into a
211 fine-mesh bag. In the laboratory, the detritus was rinsed through a 0.5 mm sieve to collect the
212 associated epifauna. Samples of algal detritus were dried at 60°C for 48 hours and the biomass was
213 calculated as dry weight /m^2.

214 Macroinfauna at the four sedimentary habitats was sampled using six sediment cores (inner
215 diameter = 5.0 cm, depth = 15 cm). The samples were sieved through a 0.5 mm sieve and animals
216 were stored in alcohol for later identification. At the seagrass sites, representative macrophyte
217 samples were collected by divers from an area around the tripod frame at the end of the deployment
218 using four randomly-placed quadrats (20 x 20 cm). The seagrass within each quadrat was gently
219 uprooted and was transferred into a net-bag. In the laboratory, the samples were rinsed through a
220 0.5 mm sieve to collect all the associated epifauna. The animals were stored in alcohol for later

identification, and the seagrass was frozen in sealed bags for further processing. The seagrass samples were later thawed, and individual shoots were counted to determine the canopy density in m^2. The above- and below-ground macrophyte biomass was separated, dried at 60°C for 48 hours and weighed.

At the rocky sites, *F. vesiculosus* individuals ($n = 4$) were randomly collected from around the instrument in fine-mesh bags. Randomly-placed quadrats (1 m^2, $n = 4$) were used to quantify the number of *F. vesiculosus* individuals per m^2. At the laboratory, the collected *F. vesiculosus* samples were carefully rinsed through a 0.5 mm sieve to collect the epifauna. The height of the *F. vesiculosus* canopy was determined from the average length of the sampled individuals. Both *F. vesiculosus* and epiphytes were separated to the extent possible, dried at 60 °C for 48 h and weighed. To collect any macrofauna on the bare rock beneath the *F. vesiculosus* canopy, Kautsky-type samplers were placed on the seafloor and the 20 cm x 20 cm area was gently scraped using a spoon into a fine-mesh sampling bag. In the laboratory, all the macrofauna from the four replicates were sieved through a 0.5 mm sieve and stored in alcohol.

The fauna from all habitats was sorted, identified to species level, counted, and weighed. The wet weight for each species was noted with 0.0001 g accuracy. In cases where the fauna occurred in very high numbers, the sample was placed in a water-filled tray and divided into eight sectors. Four sectors were randomly chosen to calculate abundance and biomass. The length of gastropods and bivalves was measured from anterior to posterior axis using Vernier callipers (accuracy = 0.01 mm) for conversion to ash-free dry mass (AFDM). The AFDM of bivalves and gastropods was calculated using established relationships between length and weight for Baltic Sea fauna (Rumohr et al., 1987).

The abundance (ind m^{-2}) and biomass (AFDM/SFDM g m^{-2}) of the invertebrates across sites were calculated. Primer (v.7 and PERMANOVA+) software was used to perform the nonmetric multidimensional scaling (nMDS, with fourth-root-transformed data) to visualize macrofauna assemblages between sites. ANOSIM based on the Bray-Curtis similarity matrix was also performed in Primer (site as a fixed factor, 4999 random sample permutations) to compare differences in macrofauna abundance and biomass between sites.

3. Results

3.1. Environmental conditions

Average water depth ranged from 2.0 m to 4.0 m at the six study sites, and average water temperature ranged from 9 °C to 16 °C during the study period (Table 1). Hypoxic conditions were only detected at the detritus site. Bottom-water [O_2] at the detritus site ranged from 1 µmol L^{-1} to 429 µmol L^{-1}, with hypoxic conditions occurring for 27 h out of the 120 h long deployment (i.e. for 23 % of the time) (Table 1). At the five other measurement sites, [O_2] were well above hypoxic conditions, with overall concentrations following diel patterns and ranging from 250 µmol L^{-1} to 490 µmol L^{-1} (Table 1).

3.2. [O_2] dynamics in detritus canopies

The [O_2] measurements within the detrital canopy document a highly dynamic [O_2] environment driven by light availability and flow velocity (Fig. 2). Within the upper layers of the canopy (i.e. ~10 to 25 cm above the seafloor), [O_2] and temporal dynamics largely follow diel patterns driven by light availability, with large ~250 µmol L^{-1} diel excursions in [O_2]. There, the [O_2] was lowest in the morning (~160 µmol L^{-1}) and highest in the evening (~430 µmol L^{-1}). In all cases, [O_2] within the upper canopy region was above hypoxic thresholds. However, under low average flow velocities < 2 cm s^{-1}, [O_2] within the lower canopy region (< 10 cm) deviated substantially from the conditions above. No diel variations in [O_2] were observed during these periods, and [O_2] rapidly became hypoxic for sustained periods (> 24 h long), with [O_2] being very low (< 10 µmol L^{-1}) during ~10 hr (~8 % of the time) (Fig. 2). As hypoxia persisted throughout the night under low flow velocities, low [O_2] extended upwards into the canopy. Hypoxic conditions ended at the onset of higher mean flow velocities of ~7 cm s^{-1}, which initiated a rapid (i.e. within 1.5 hr) oxygenation of the entire canopy.

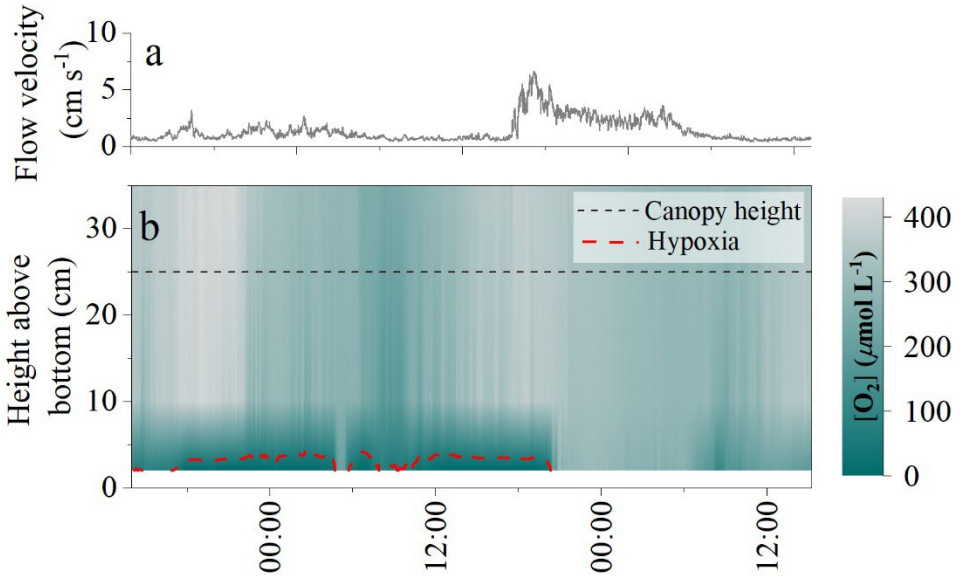

Fig. 2: (a) Flow velocity measured by the velocimeter 10 cm above the detritus canopy and (b) O_2 distribution within the canopy as resolved by three O_2 sensors located at 3 cm, 10 cm, and 35 cm above the seafloor. Deployment starting from 29th May 2018.

3.3. Pulses of hypoxic waters

High-frequency [O_2] measurements performed 10 cm above the detritus canopy document transient pulses of hypoxic water originating from within the canopy and propagating upwards into the water column (Fig 3). Such pulses typically followed quiescent weather and occurred at the onset of increased flow velocities. It took < 1 min to reduce [O_2] in the water column from 220 µmol L^{-1} to 65 µmol L^{-1}. Subsequently, a recovery period followed where [O_2] gradually increased back to previous concentrations over a ~5 min period. These rapid variations in water column [O_2] were not captured by the slow-response [O_2] optode sampling at 1 min intervals.

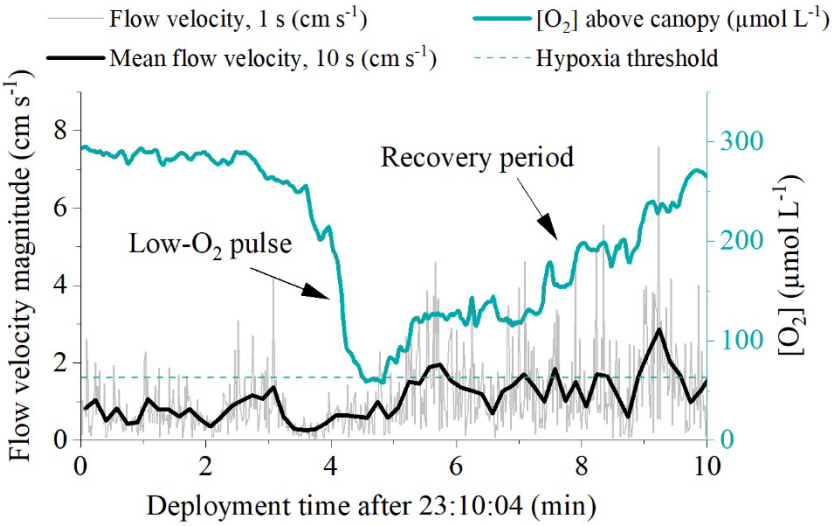

Figure 3: High-frequency [O_2] measured 10 cm above the detrital canopy documented pulses of hypoxic water originating from within the canopy and propagating upwards into the water column. Data from 20th September 2017.

3.4. Benthic O_2 fluxes and detritus metabolic rates

The eddy covariance measurements at the detritus site produced three days of continuous flux data in June 2017, three days of data in September 2017, and five days of data in May 2018. Benthic O_2 fluxes documented a dynamic O_2 exchange rate driven by light availability and flow velocity. During quiescent periods with low flow velocity < 2 cm s^{-1}, a clear diel signal in the O_2 flux was observed, indicating substantial primary production associated to the detritus canopy. Higher flow velocities stimulated O_2 uptake rates by up to 5-fold, indicating that canopy ventilation through mixing increased O_2 uptake.

Hourly O_2 fluxes ranged from -22 mmol O_2 m^{-2} h^{-1} at night to 13 mmol O_2 m^{-2} h^{-1} during the day and showed a distinct diel cycle in response to sunlight availability (Fig. 4). Daily R ranged from 26 to 97 mmol O_2 m^{-2} d^{-1}, and daily GPP was between 15 and 74 mmol O_2 m^{-2} d^{-1}. Daily R exceeded GPP in all 11 measurement days (net heterotrophic), with NEM ranging from -7 to -32 mmol O_2 m^{-2} d^{-1} (Fig. 4, Table A1). The deployment average (± SD) GPP:R for the detritus canopy was 0.77 ± 0.04 in June 2017 (n = 3), 0.55 ± 0.02 in September 2017 (n = 3), and 0.77 ± 0.00 in May 2018 (n = 5), and the global mean GPP:R was 0.71 ± 0.11 (n = 11).

There was a significant positive relationship between daily detritus GPP and R in all measurement campaigns, with the detritus canopy seemingly becoming more heterotrophic (i.e. R > GPP) as the

magnitude of the metabolic rates increased (Fig. 5, Table A1). Significant positive relationships were also observed between daily detritus GPP and daily seabed PAR (Table A1). Canopy light-use efficiency (LUE), estimated as the ratio between daily GPP and daily PAR (Attard and Glud, 2020), was 0.004 O_2 photon^{-1} in June 2017, 0.006 O_2 photon^{-1} in September 2017, and 0.004 O_2 photon^{-1} in May 2018 (Table A1).

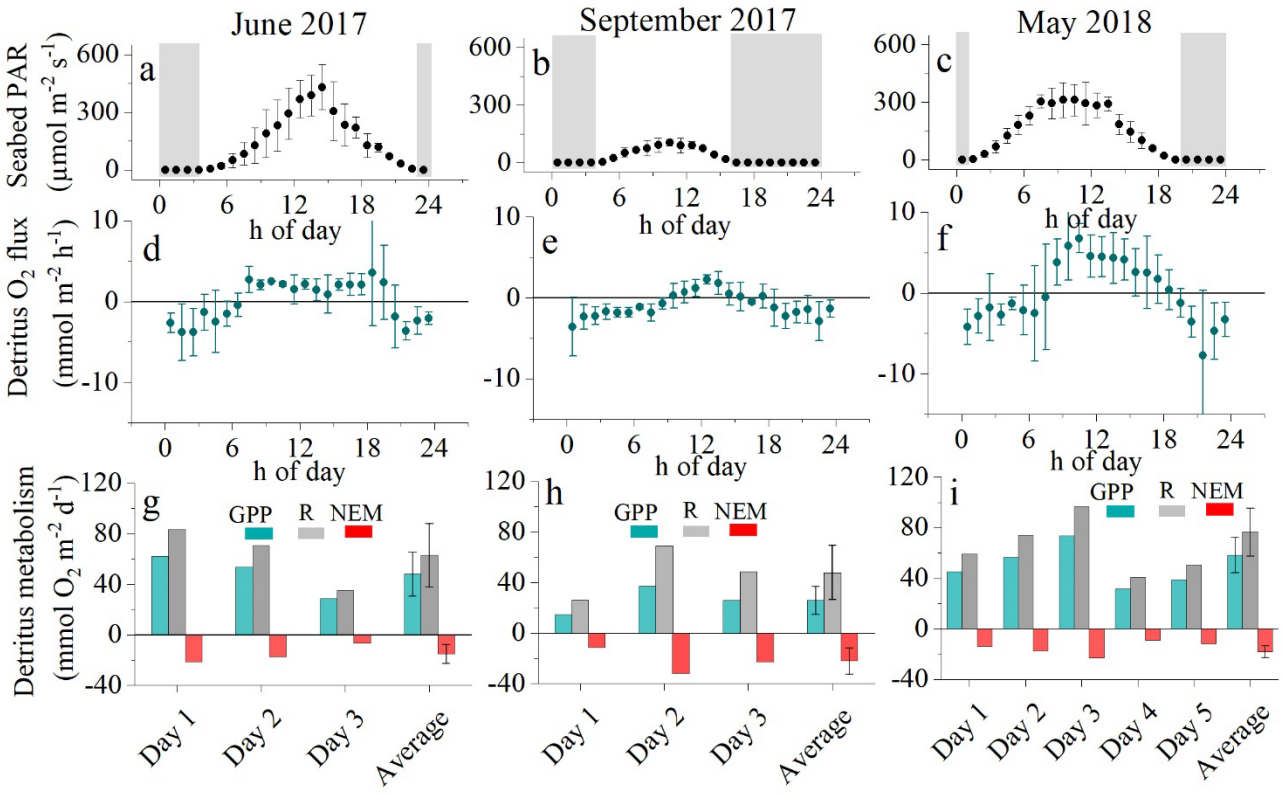

Fig. 4: Hourly seabed PAR (a, b, c) with night-time periods grey shaded, hourly O_2 fluxes (d, e, f) and daily metabolism estimates of gross primary production (GPP), respiration (R), and net ecosystem metabolism (NEM) for the detritus canopy for the three measurement campaigns (g, h, i). Seabed PAR and O_2 fluxes are shown as mean ± 1 s.d. and are binned by the hour of day.

There was a significant positive relationship between near-bed incident PAR and the benthic O_2 flux (Fig. 5). Light-saturation curves fitted to hourly data from all deployments indicated a maximum gross primary production rate (P_m) of 5.14 ± 0.56 mmol O_2 m^{-2} h^{-1}, an α of 0.03 ± 0.01, and a R rate of 1.92 ± 0.26 mmol O_2 m^{-2} h^{-1}. Light saturation (I_k) of the detritus canopy occurred at irradiances greater than ~170 µmol PAR m^{-2} s^{-1}.

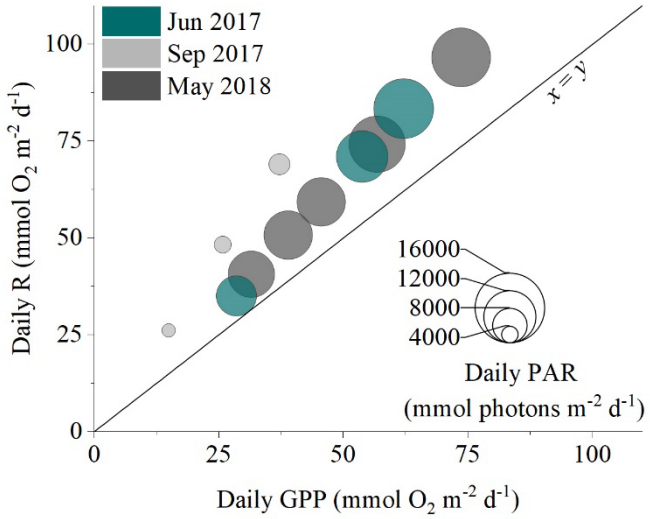

Fig. 5: The daily balance between detritus gross primary production (GPP) and respirati®(R) for the three measurement campaigns. Symbol size corresponds to the daily integrated PAR reaching the seafloor.

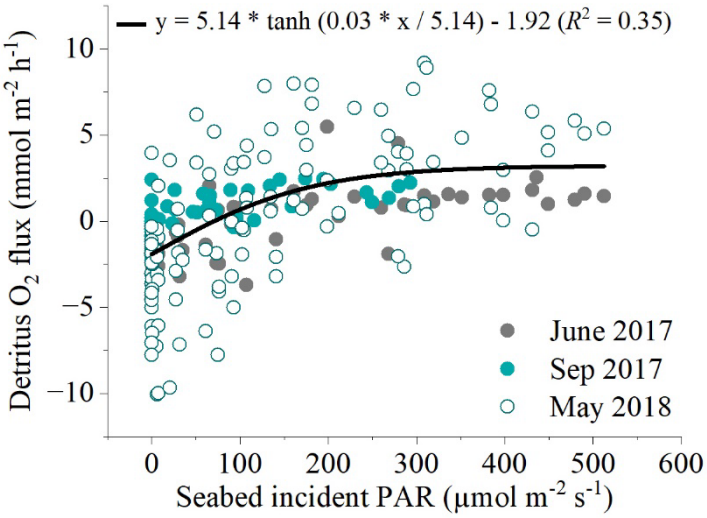

Fig. 6: Relationship between all hourly in situ benthic O_2 fluxes at the detritus site and light availability from the three flux datasets measured. A modified photosynthesis-irradiance curve by Platt et al. (1980) is shown as the line-of-best-fit to the global dataset.

3.5. Macrobenthic diversity and abundance

The detritus site had a biomass of accumulated macrophyte (*F. vesiculosus*) detritus of 1666 ± 223 g dry weight m^{-2} (mean ± SE, $n = 4$), approximately 1.5-fold larger than nearby intact *F. vesiculosus*

canopies (Table 2). Detritus accumulation in the five other habitats was around 100-fold smaller. The area of the detritus site estimated using Google Earth was 2300 m^2, amounting to 3,800 kg dry weight of *F. vesiculosus* fragments. Macrofauna abundance ranged from 2700 ± 900 ind. m^{-2} at the bare sediments site to 17300 ± 2400 ind. m^{-2} at the sheltered *F. vesiculosus* site (mean ± SE, $n = 4$) (Table 3). Macrofauna biomass ranged from 6 ± 2 g m^{-2} at the bare site to 41 ± 9 g m^{-2} at the exposed seagrass site (mean ± SE, $n = 4$), and the number of species ranged from 6 to 23, with the lowest values measured at the bare sediments and detritus sites, and the highest values at the sheltered *F. vesiculosus* site (Table 3).

At the detritus site, there was a low abundance of epifaunal crustaceans when compared to other habitats with canopies. Key species, such as the amphipod *Gammarus spp.* were notably absent, and isopods such as *Idotea spp.* were present in low abundance (Table A3). Similarly, there was a notable absence of bivalves such as the soft-shelled clam, *Mya arenaria*, and the cockle *Cerastoderma glaucum*. Polychaetes such as *Hediste diversicolor* and *Marenzelleria spp*. were also absent from the detritus site but present in other sedimentary habitats (Table A3). The nMDS ordination of the macrofaunal assemblages indicated a clear separation of points representing the different habitat sites (ANOSIM: $R^2 = 0.865$; $p < 0.001$). The assemblages from the bare sand and the detritus sites formed separated site groupings compared to the vegetated sites ('*Fucus*' and 'seagrass', both exposed and sheltered). Within the vegetated sites, the assemblages of the 'seagrass sheltered' and the '*Fucus* sheltered' sites were the most different (Fig. 7).

355 Table 2: Vegetation abundance and biomass (dry weight) at the six study sites. Abundance is shoots
356 per m^2 for seagrass and individuals per m^2 for *F. vesiculosus*. Values are mean ± SE.

Site	Abundance per m^2	Above-ground biomass (g m^{-2})	Belowground biomass (g m^{-2})	Detritus (g m^{-2})	Biomass other species (g m^{-2})
Macrophyte detritus	-	-	-	1666 ± 223	-
Bare sediments	-	-	-	-	-
Sheltered *Z. marina*	768 ± 92	21 ± 2	8 ± 1	58 ± 13	0.1 ± 0.1
Exposed *Z. marina*	2565 ± 164	69 ± 7	25 ± 3	16 ± 2	0.2 ± 0.2
Sheltered *F. vesiculosus*	16 ± 2	1244 ± 58	-	55 ± 11	-
Exposed *F. vesiculosus*	16 ± 2	1112 ± 119	-	20 ± 2	-

357

358 Table 3: Macrofauna abundance, biomass (ash-free dry weight), and number of species at the six
359 study sites.

Site	Infauna abundance (ind. m^{-2})	Epifauna abundance (ind. m^{-2})	Total abundance (ind. m^{-2})	Infauna biomass (g m^{-2})	Epifauna biomass (g m^{-2})	Total biomass (g m^{-2})	Number of species
Macrophyte detritus	4175 ± 2885	493 ± 37	4668 ± 2885	5 ± 3	5 ± 0	9 ± 3	6
Bare sediments	2719 ± 854	-	2719 ± 854	6 ± 2	-	6 ± 2	6
Sheltered *Z. marina*	6110 ± 787	3020 ± 874	9130 ± 1176	30 ± 6	2 ± 0	33 ± 6	18
Exposed *Z. marina*	6959 ± 620	3316 ± 772	10275 ± 990	31 ± 8	10 ± 2	41 ± 9	16
Sheltered *F. vesiculosus*	-	17259 ± 2421	17259 ± 2421	-	11 ± 2	11 ± 2	23
Exposed *F. vesiculosus*	-	3551 ± 609	3551 ± 609	-	7 ± 2	7 ± 2	12

360

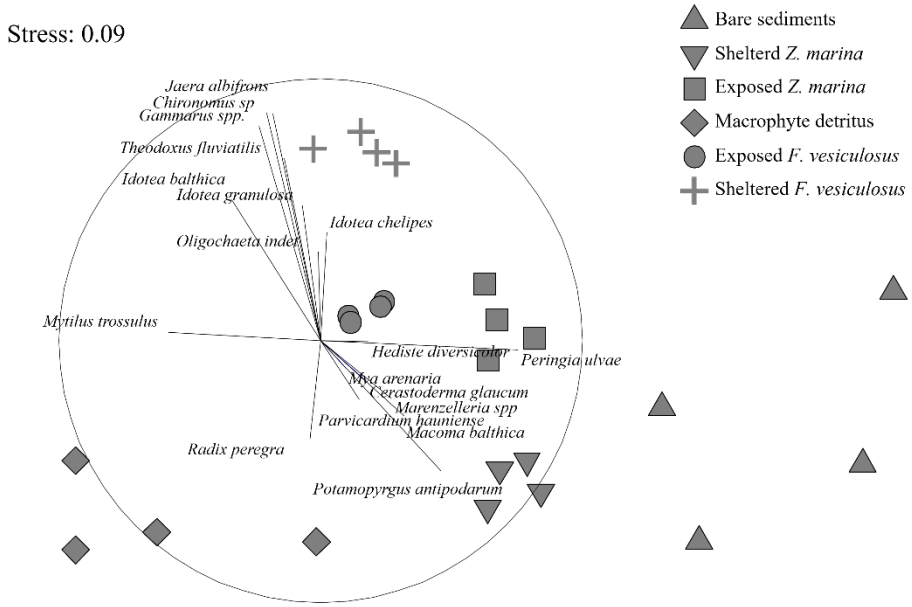

361

362 Fig. 7: A non-metric multidimensional scaling (nMDS) ordination of the macrofaunal assemblages
363 indicated a clear separation of points representing the different habitat sites. The assemblages from
364 the bare sand and the detritus sites formed separate site groupings compared to the vegetated sites.
365 Data from May/June 2018 (see Table 1).

366 **4. Discussion**

367 *4.1. Detritus metabolism*

368 The eddy covariance measurements document a highly active detrital canopy that photosynthesized
369 as well as respired. High daily rates of GPP of up to 75 mmol O_2 m^{-2} d^{-1} and R of 100 mmol O_2 m^{-2}
370 d^{-1} are comparable to some of the most productive habitats in the area, such as dense seagrass
371 meadows (*Zostera marina*) and intact canopies of bladder wrack (*Fucus vesiculosus*) (Attard et al.,
372 2019b). However, intact canopies of *F. vesiculosus* function very differently to detritus canopies
373 from a metabolic standpoint. In June 2017, two eddy covariance instruments were deployed in
374 parallel: one at the detritus site, and another at a nearby intact canopy. While the detritus was net
375 heterotrophic (NEM = -15 mmol O_2 m^{-2} d^{-1}; GPP:R = 0.76), the intact *F. vesiculosus* canopy was
376 strongly net autotrophic (NEM = 167 mmol O_2 m^{-2} d^{-1}; GPP:R = 6.40) (Attard et al., 2019b). Daily
377 R at the detritus site was up to ~5-fold larger than that at a nearby (within 4 km) site with bare
378 sediments and up to twice as high as a neighbouring intact canopy of *F. vesiculosus* (Attard et al.,
379 2019b). Decaying (and respiring) fragments of *F. vesiculosus* could contribute substantially to the
380 O_2 uptake rate: laboratory incubations of *F. vesiculosus* fragments resolved respiration rates ~5

381 µmol O_2 g dw^{-1} h^{-1}, equivalent to ~25 mmol O_2 m^{-2} d^{-1} when upscaled to *in situ* biomass observed at
382 the detritus site (data not shown).

383 Notwithstanding the key metabolic differences between detritus and other neighbouring sites, the
384 flux measurements (Figure 4) indicate that shallow detritus accumulation zones are not just regions
385 of organic matter remineralization, but rather they synthesize substantial amounts of organic matter
386 through primary production. The range in daily GPP:R from 0.53 to 0.81 indicates that primary
387 production can offset a substantial proportion of the respiratory demand, which extends the
388 persistence of detritus in the coastal zone. These observations are consistent with the laboratory
389 study by Frontier et al. (2021), who determined that following detachment, kelp (*Laminaria*
390 *hyperborea* and *L. ochroleuca*) fragments retain physiological and reproductive capabilities for up
391 to several months. Carbon retention within the coastal zone and export to deeper, sedimentary
392 accumulation regions would therefore be larger than would be predicted by decomposition theory
393 alone. Similarly, slow, and incomplete degradation of algae detritus under low [O_2] conditions,
394 which could occur, for instance, in the bottom layers of detrital canopies or in the large anoxic
395 basins of the Baltic Sea (Conley et al., 2009), would increase carbon retention, transfer, and
396 sequestration potential (Pedersen et al., 2021).

397 *4.2. Periodic benthic hypoxia*

398 Our in situ measurements performed over a few days in late spring document that subtidal detritus
399 accumulation zones uniquely experience dynamic [O_2] conditions driven by sunlight availability
400 and flow velocity, with rapid [O_2] oscillations and frequent periods of hypoxia (Table 1). Hypoxic
401 conditions were largely restricted to the lower ~5 cm of the canopy and were only revealed by
402 sensors placed directly above the sediment surface (< 5 cm distance). At the onset of wave-driven
403 mixing, hypoxic waters from within the canopy propagated upwards into the water column and
404 were registered by fast-response [O_2] sensors located 10 cm above the canopy (~35 cm above the
405 seafloor). This observation suggests that the [O_2] conditions inside the entire canopy and even in the
406 water column directly above can reach hypoxic conditions for a few minutes (Fig. 3). Such pulses,
407 however, were not registered by the slow-response [O_2] optodes with a factory-specified T_{90} < 2
408 min. The minimum [O_2] observed by these sensors placed at 10 cm and 35 cm above the seafloor
409 was 158 and 229 µmol L^{-1}, respectively, and thus well above hypoxic conditions.

410 The importance of measuring [O_2] close to the seafloor was demonstrated more than 40 years ago
411 by Jorgensen (1980), and since then, other researchers have investigated the distribution of

412 dissolved constituents such as O_2 and nutrients in the benthic boundary layer (Holtappels et al.,
413 2011). These studies document that solute gradients are largest near the seafloor. For practical
414 reasons, however, coastal monitoring programs measure [O_2] further away from the seafloor.
415 Models based on monitoring data suggest that hypoxia is prevalent in only small areas of the
416 shallow subtidal zone. For instance, models for the northern Baltic Sea, which cover a total seabed
417 area of 12435 km^2 of which 2211 km^2 is in shallow waters <5 m depth, indicate that just 16.5 km^2
418 (or 0.75% of shallow waters) are prone to hypoxia (Virtanen et al., 2019). Given that large
419 quantities of drifting macrophytes are a common phenomenon in the shallow subtidal zone of the
420 northern Baltic Sea (Norkko and Bonsdorff, 1996a), it is likely that coastal hypoxia is currently
421 underestimated because large-scale models are largely based on measurements performed higher
422 above the seafloor (0.5-1.0 m) (Virtanen et al., 2019; Conley et al., 2011).

423 *4.3. Biodiversity and [O_2] dynamics in detritus canopies*

424 Despite being considered a temporary habitat, detritus was found in abundance at our study site on
425 all occasions in May, June, and September. This type of habitat is likely quite widespread in the
426 Baltic. Habitat distribution models for the area indicate a dominance of *F. vesiculosus* canopies in
427 shallow waters < 5 m depth (Virtanen et al., 2018), and these canopies are expected to export
428 substantial amounts of organic matter (~0.3 kg C m^{-2} yr^{-1}) which can accumulate in topographical
429 depressions with limited water exchange (Attard et al., 2019a). Topographic depressions occupy
430 ~1350 km^2 or ~11% of the northern Baltic Sea (Virtanen et al., 2019). During a recent seasonal
431 study, we observed the highest abundance of detritus at our study site in summer and autumn,
432 coinciding with high southerly winds that erode intact canopies in shallower waters (Attard et al.,
433 2019a). However, we also observed significant canopy erosion in winter when a substantial biomass
434 of *F. vesiculosus* froze into sea ice and got dislodged once the ice broke up (Fig. 7). Therefore,
435 some degree of drifting detritus might be common throughout the year. Drifting detritus constitutes
436 a significant habitat structure. Given high enough biomass, however, detritus canopies can be a
437 challenging habitat for most species. At our study site, hypoxic conditions uniquely occurred at the
438 detritus site and for around a quarter of the deployment time (Table 1). We can expect these
439 conditions to be particularly challenging for crustaceans, the most hypoxia-sensitive
440 macroinvertebrate group (Vaquer-Sunyer and Duarte, 2008). Indeed, we only found one crustacean
441 species at this site- the isopod *Idotea balthica* (Table A3)- which is mobile and can tolerate hypoxic
442 conditions for a few hours (Vetter and Dayton, 1999). All other invertebrates observed at the
443 detritus site were mollusks (Table A3), the most hypoxia-tolerant marine invertebrate group

(Vaquer-Sunyer and Duarte, 2008). Other tolerant species include the blue mussel *Mytilus trossulus x edulis* that can survive > 300 h of anoxia (Jorgensen, 1980), although the survival of larvae depends on its developmental stage (Diaz and Rosenberg, 1995). Similarly, the mudsnail *Peringia ulvae* is highly mobile and can survive > 150 h of anoxia (Jorgensen, 1980; Norkko et al., 2000).

Overall, the dynamic [O_2] conditions in detrital canopies seem to be challenging for most species in this region of the Baltic Sea, with lethal and non-lethal thresholds frequently being exceeded on timescales of hours to days. We currently have a poor understanding of the extent of periodic hypoxia in coastal waters, because [O_2] measurements are performed at some distance away from the seabed. While this is a practical approach that is done to minimize sensor fouling and damage, it does not reveal the full extent of coastal hypoxia. If implemented widely, sensor arrays, as described herein, and sensor elevators (e.g. (Holtappels et al., 2011)) can fill in this knowledge gap and provide important insights into the ecological status and biogeochemical cycling that is needed for the sustainable management of coastal ecosystems.

Fig. 8: substantial detritus accumulation was observed in late winter (March 2021) when *F. vesiculosus* froze into sea ice and got dislodged once the ice broke up. (Photo by Alf Norkko)

461 Table A1: A summary of the eddy covariance flux measurements performed on the detritus canopy
462 during the three measurement campaigns. Daily integrated seabed PAR and detritus light-use
463 efficiency (LUE, calculated as daily GPP/ daily PAR) are also presented.

Field campaign	Day	Daily GPP (mmol O_2 m^{-2} d^{-1})	Daily R (mmol O_2 m^{-2} d^{-1})	GPP:R	Daily PAR (mmol photons m^{-2} d^{-1})	LUE (O_2 $photon^{-1}$)
Jun 2017	1	62	83	0.74	13554	0.005
	2	54	71	0.76	11710	0.005
	3	29	35	0.81	9044	0.003
Sep 2017	1	15	26	0.57	3013	0.005
	2	37	69	0.54	4827	0.008
	3	26	48	0.53	3815	0.007
May 2018	1	46	59	0.77	10997	0.004
	2	57	74	0.76	12732	0.004
	3	74	97	0.76	13336	0.006
	4	32	41	0.78	10523	0.003
	5	39	51	0.77	10915	0.004

464

465

Table A2: Fit statistics for linear regressions performed between daily detritus GPP and R, and daily GPP and benthic PAR. Where relevant, values are presented ± SE. The SE was scaled with the square root of the reduced Chi-Sqr. ANOVA was used to test slope significance. Asterisks indicate that the slope was significantly different from zero at the 0.05 level.

Relationship between daily GPP and daily R				
Field campaign	Slope of linear regression ± SE	Intercept ± SE	R^2	ANOVA Prob > F
Jun 2017	1.43 ± 0.02	-5.91 ± 0.77	0.99	0.01*
Sep 2017	1.93 ± 0.06	-2.19 ± 1.70	0.99	0.02*
May 2018	1.33 ± 0.00	-1.09 ± 0.17	0.99	0.00*
Global	1.16 ± 0.13	9.90 ± 5.92	0.89	0.00*
Relationship between daily GPP and daily PAR				
Field campaign	Slope of linear regression ± SE	Intercept ± SE	R^2	ANOVA Prob > F
Jun 2017	128 ± 23	5293 ± 1164	0.94	0.11
Sep 2017	82 ± 4	1765 ± 121	0.99	0.03*
May 2018	73 ± 12	8103 ± 609	0.90	0.01*
Global	182 ± 40	1725 ± 1852	0.66	0.00*

472 Table A3: Species list for the five studied sites. Presence is indicated by 'x'.

Group	Species	Macrophyte detritus	Bare sediments	Sheltered *Z. marina*	Exposed *Z. marina*	Sheltered *F. vesiculosus*	Exposed *F. vesiculosus*
Crustacea	*Amphibalanus improvisus*			x			
	Asellus aquaticus					x	
	Corophium spp.			x			
	Gammarus spp.			x	x	x	x
	Idotea balthica	x			x	x	x
	Idotea chelipes				x	x	x
	Idotea granulosa			x	x	x	x
	Jaera albifrons			x	x	x	x
	Cladocera					x	
	Copepoda					x	
	Ostracoda sp.					x	
	Mysid					x	x
Bivalvia	*Cerastoderma glaucum*			x	x		
	Parvicardium haunience			x	x		
	Macoma balthica	x	x	x	x	x	x
	Mya arenaria			x	x		
	Mytilus trossulus x edulis	x		x	x	x	x
Gastropoda	*Peringia ulvae*	x	x	x	x	x	x
	Radix sp.	x		x			x
	Potamopyrgus antipodarum		x	x			
	Theodoxus fluviatilis	x	x	x	x	x	x

Polychaeta	*Hediste diversicolor*			x	x		
	Halicryptus spinulosus					x	
	Maranzelleria spp.		x	x	x	x	
	Nematoda					x	
	Oligochaeta			x	x	x	
	Pygospio elegans					x	
Others	*Chironomus* sp			x	x	x	x
	Coleoptera larvae						x
	Odonata						x
	Cyanophthalma obscura						x
	Hydrachnidae		x				x

473

Author contribution

All authors contributed significantly to designing the research, funding the study, collecting the data, analyzing samples and data, and interpreting the results. KMA wrote the paper with input from all authors.

Competing interests

The authors declare that they have no conflict of interest

Data availability

All data presented in this paper will be made available in a FAIR-aligned data repository upon acceptance of the paper.

Acknowledgements

Colleagues at the Tvärminne Zoological Station provided help with fieldwork and logistics. Anni Glud at the University of Southern Denmark constructed the oxygen microsensors used in this study. Elina Virtanen at the Finnish Environmental Institute (SYKE) provided spatial data used to estimate the potential extent of detritus canopies. The Walter and Andrée de Nottbeck Foundation supported this work through a postdoctoral fellowship to KMA and through a Masters fellowship to AL. Further funding for this project was provided by research grants from the Academy of Finland (project ID 294853), the University of Helsinki and Stockholm University strategic fund for collaborative research (the Baltic Bridge initiative), and Denmark's Independent Research Fund (project ID 7014-00078). This study has utilized research infrastructure facilities provided by FINMARI (Finnish Marine Research Infrastructure network, The Academy of Finland, project ID 283417).

References

Attard, K. M. and Glud, R. N.: Technical Note: Estimating light-use efficiency of benthic habitats using underwater O-2 eddy covariance, Biogeosciences, 17, 4343-4353, 2020.

Attard, K. M., Rodil, I. F., Berg, P., Norkko, J., Norkko, A., and Glud, R. N.: Seasonal metabolism and carbon export potential of a key coastal habitat: The perennial canopy-forming macroalga *Fucus vesiculosus*, Limnol Oceanogr, 64, 149-164, 10.1002/lno.11026, 2019a.

Attard, K. M., Rodil, I. F., Glud, R. N., Berg, P., Norkko, J., and Norkko, A.: Seasonal ecosystem metabolism across shallow benthic habitats measured by aquatic eddy covariance, Limnology and Oceanography Letters, 4, 79-86, 10.1002/lol2.10107, 2019b.

Berg, P. and Pace, M. L.: Continuous measurement of air-water gas exchange by underwater eddy covariance, Biogeosciences, 14, 5595-5606, 2017.

Berg, P., Røy, H., and Wiberg, P. L.: Eddy correlation flux measurements: the sediment surface area that contributes to the flux, Limnol Oceanogr, 52, 1672-1684, 10.4319/lo.2007.52.4.1672, 2007.

Berg, P., Huettel, M., Glud, R. N., Reimers, C. E., and Attard, K. M.: Aquatic Eddy Covariance: The Method and Its Contributions to Defining Oxygen and Carbon Fluxes in Marine Environments, Annual Review of Marine Science, 14, 431-455, 10.1146/annurev-marine-042121-012329, 2022.

Berg, P., Røy, H., Janssen, F., Meyer, V., Jorgensen, B. B., Huettel, M., and de Beer, D.: Oxygen uptake by aquatic sediments measured with a novel non-invasive eddy-correlation technique, Marine Ecology Progress Series, 261, 75-83, 10.3354/Meps261075, 2003.

Bittig, H. C., Kortzinger, A., Neill, C., van Ooijen, E., Plant, J. N., Hahn, J., Johnson, K. S., Yang, B., and Emerson, S. R.: Oxygen Optode Sensors: Principle, Characterization, Calibration, and Application in the Ocean, Frontiers in Marine Science, 4, 2018.

Breitburg, D., Levin, L. A., Oschlies, A., Gregoire, M., Chavez, F. P., Conley, D. J., Garcon, V., Gilbert, D., Gutierrez, D., Isensee, K., Jacinto, G. S., Limburg, K. E., Montes, I., Naqvi, S. W. A., Pitcher, G. C., Rabalais, N. N., Roman, M. R., Rose, K. A., Seibel, B. A., Telszewski, M., Yasuhara, M., and Zhang, J.: Declining oxygen in the global ocean and coastal waters, Science, 359, 46-+, 2018.

Broch, O. J., Hancke, K., and Ellingsen, I. H.: Dispersal and Deposition of Detritus From Kelp Cultivation, Frontiers in Marine Science, 9, 2022.

Broch, O. J., Alver, M. O., Bekkby, T., Gundersen, H., Forbord, S., Handa, A., Skjermo, J., and Hancke, K.: The Kelp Cultivation Potential in Coastal and Offshore Regions of Norway, Frontiers in Marine Science, 5, 2019.

Camillini, N., Attard, K. M., Eyre, B. D., and Glud, R. N.: Resolving community metabolism of eelgrass Zostera marina meadows by benthic flume-chambers and eddy covariance in dynamic coastal environments, Marine Ecology Progress Series, 661, 97-114, 2021.

Carstensen, J. and Conley, D. J.: Baltic Sea Hypoxia Takes Many Shapes and Sizes, Limnology and Oceanography Bulletin, 28, 125-129, https://doi.org/10.1002/lob.10350, 2019.

Conley, D. J., Carstensen, J., Aigars, J., Axe, P., Bonsdorff, E., Eremina, T., Haahti, B. M., Humborg, C., Jonsson, P., Kotta, J., Lannegren, C., Larsson, U., Maximov, A., Medina, M. R., Lysiak-Pastuszak, E., Remeikaite-Nikiene, N., Walve, J., Wilhelms, S., and Zillen, L.: Hypoxia Is Increasing in the Coastal Zone of the Baltic Sea, Environ Sci Technol, 45, 6777-6783, 10.1021/es201212r, 2011.

Conley, D. J., Bjorck, S., Bonsdorff, E., Carstensen, J., Destouni, G., Gustafsson, B. G., Hietanen, S., Kortekaas, M., Kuosa, H., Meier, H. E. M., Muller-Karulis, B., Nordberg, K., Norkko, A., Nurnberg, G., Pitkanen, H., Rabalais, N. N., Rosenberg, R., Savchuk, O. P., Slomp, C. P., Voss, M., Wulff, F., and Zillen, L.: Hypoxia-Related Processes in the Baltic Sea, Environ Sci Technol, 43, 3412-3420, 10.1021/es802762a, 2009.

Davanzo, C. and Kremer, J. N.: Diel Oxygen Dynamics and Anoxic Events in an Eutrophic Estuary of Waquoit Bay, Massachusetts, Estuaries, 17, 131-139, 1994.

Diaz, R. J. and Rosenberg, R.: Marine benthic hypoxia: A review of its ecological effects and the behavioural responses of benthic macrofauna, Oceanography and Marine Biology - an Annual Review, Vol 33, 33, 245-303, 1995.

Diaz, R. J. and Rosenberg, R.: Spreading dead zones and consequences for marine ecosystems, Science, 321, 926-929, 10.1126/science.1156401, 2008.

Duarte, C. M. and Cebrián, J.: The fate of marine autotrophic production, Limnol Oceanogr, 41, 1758-1766, DOI 10.4319/lo.1996.41.8.1758, 1996.
Fenchel, T. and Glud, R. N.: Benthic primary production and O2-CO2 dynamics in a shallow-water sediment: Spatial and temporal heterogeneity, Ophelia, 53, 159-171, 2000.
Frontier, N., de Bettignies, F., Foggo, A., and Davoult, D.: Sustained productivity and respiration of degrading kelp detritus in the shallow benthos: Detached or broken, but not dead, Mar Environ Res, 166, 2021.
Garcia, H. E. and Gordon, L. I.: Oxygen Solubility in Seawater - Better Fitting Equations, Limnol Oceanogr, 37, 1307-1312, 1992.
Glud, R. N.: Oxygen dynamics of marine sediments, Mar Biol Res, 4, 243-289, 2008.
Glud, R. N., Rysgaard, S., Fenchel, T., and Nielsen, P. H.: A conspicuous H2S-oxidizing microbial mat from a high-latitude Arctic fjord (Young Sound, NE Greenland), Mar Biol, 145, 51-60, DOI 10.1007/s00227-004-1296-8, 2004.
Holtappels, M., Kuypers, M. M. M., Schluter, M., and Bruchert, V.: Measurement and interpretation of solute concentration gradients in the benthic boundary layer, Limnol Oceanogr-Meth, 9, 1-13, 2011.
Jorgensen, B. B.: Seasonal Oxygen Depletion in the Bottom Waters of a Danish Fjord and Its Effect on the Benthic Community, Oikos, 34, 68-76, 1980.
Juska, I. and Berg, P.: Variation in seagrass meadow respiration measured by aquatic eddy covariance, Limnology and Oceanography Letters, 7, 410-418, https://doi.org/10.1002/lol2.10276, 2022.
Krumhansl, K. A. and Scheibling, R. E.: Production and fate of kelp detritus, Marine Ecology Progress Series, 467, 281-302, 10.3354/meps09940, 2012.
Long, M. H. and Nicholson, D. P.: Surface gas exchange determined from an aquatic eddy covariance floating platform, Limnol Oceanogr-Meth, 16, 145-159, 2018.
McGinnis, D. F., Cherednichenko, S., Sommer, S., Berg, P., Rovelli, L., Schwarz, R., Glud, R. N., and Linke, P.: Simple, robust eddy correlation amplifier for aquatic dissolved oxygen and hydrogen sulfide flux measurements, Limnol Oceanogr-Meth, 9, 340-347, DOI 10.4319/lom.2011.9.340, 2011.
Middelburg, J. J. and Levin, L. A.: Coastal hypoxia and sediment biogeochemistry, Biogeosciences, 6, 1273-1293, DOI 10.5194/bg-6-1273-2009, 2009.
Norkko, A. and Bonsdorff, E.: Population responses of coastal zoobenthos to stress induced by drifting algal mats, Marine Ecology Progress Series, 140, 141-151, DOI 10.3354/meps140141, 1996a.
Norkko, A. and Bonsdorff, E.: Rapid zoobenthic community responses to accumulations of drifting algae, Marine Ecology Progress Series, 131, 143-157, DOI 10.3354/meps131143, 1996b.
Norkko, J., Bonsdorff, E., and Norkko, A.: Drifting algal mats as an alternative habitat for benthic invertebrates: Species specific responses to a transient resource, Journal of Experimental Marine Biology and Ecology, 248, 79-104, 2000.
Pedersen, M. F., Filbee-Dexter, K., Frisk, N. L., Sarossy, Z., and Wernberg, T.: Carbon sequestration potential increased by incomplete anaerobic decomposition of kelp detritus, Marine Ecology Progress Series, 660, 53-67, 2021.
Platt, T., Gallegos, C. L., and Harrison, W. G.: Photoinhibition of photosynthesis in natural assemblages of marine phytoplankton, J Mar Res, 38, 687-701, 1980.
Rheuban, J. E., Berg, P., and McGlathery, K. J.: Multiple timescale processes drive ecosystem metabolism in eelgrass (*Zostera marina*) meadows, Marine Ecology Progress Series, 507, 1-13, 10.3354/meps10843, 2014.
Robertson, E. K., Roberts, K. L., Burdorf, L. D. W., Cook, P., and Thamdrup, B.: Dissimilatory nitrate reduction to ammonium coupled to Fe(II) oxidation in sediments of a periodically hypoxic estuary, Limnol Oceanogr, 61, 365-381, 2016.
Rodil, I. F., Attard, K. M., Norkko, J., Glud, R. N., and Norkko, A.: Towards a sampling design for characterizing habitat-specific benthic biodiversity related to oxygen flux dynamics using Aquatic Eddy Covariance, Plos One, 14, e0211673, 10.1371/journal.pone.0211673, 2019.
Rumohr, H., Brey, T., and Ankar, S.: A compilation of biometric conversion factors for benthic invertebrates of the Baltic Sea, Baltic Marine Biologists, 9, 1-56, 1987.

595 Smith, S. V.: Marine macrophytes as a global carbon sink, Science, 211, 838-840, DOI
596 10.1126/science.211.4484.838, 1981.
597 Tyler, R. M., Brady, D. C., and Targett, T. E.: Temporal and Spatial Dynamics of Diel-Cycling Hypoxia in
598 Estuarine Tributaries, Estuar Coast, 32, 123-145, 10.1007/s12237-008-9108-x, 2009.
599 Vaquer-Sunyer, R. and Duarte, C. M.: Thresholds of hypoxia for marine biodiversity, P Natl Acad Sci USA,
600 105, 15452-15457, 10.1073/pnas.0803833105, 2008.
601 Vetter, E. W. and Dayton, P. K.: Organic enrichment by macrophyte detritus, and abundance patterns of
602 megafaunal populations in submarine canyons, Marine Ecology Progress Series, 186, 137-148, 1999.
603 Virtanen, E., Viitasalo, M., Lappalainen, J., and Moilanen, A.: Evaluation, gap analysis, and potential
604 expansion of the Finnish marine protected area network, Frontiers in Marine Science,
605 10.3389/fmars.2018.00402, 2018.
606 Virtanen, E. A., Norkko, A., Sandman, A. N., and Viitasalo, M.: Identifying areas prone to coastal hypoxia -
607 the role of topography, Biogeosciences, 16, 3183-3195, 2019.

608